Proc. of the European Safety and Reliability Conference (ESREL 2026)
Edited by José C. Matos, Paulo B. Lourenço, Michael Beer, Daniel Oliveira,
Edoardo Patelli, Hélder S. Sousa, Rui A. Silva and Monica Santamaria
 Published by Research Publishing, Singapore.
doi: 10.3850/ESREL2026061419_esrel26-p27671-cd

Machine Learning-Based Structural Reliability of Freeform Thin Concrete Shells

Bárbara Gomes

NOVA School of Science and Technology, NOVA University Lisbon, Portugal. E-mail: bcgomes.eng@gmail.com

Eduardo Cavaco

NOVA School of Science and Technology, NOVA University Lisbon, Portugal. E-mail: e.cavaco@fct.unl.pt

Joana Vanzeller

NOVA School of Science and Technology, NOVA University Lisbon, Portugal. E-mail: j.vanzeller@campus.fct.unl.pt

This study presents a reliability assessment of an unreinforced prefabricated funicular concrete shell designed for membrane-dominated behaviour under uniform loading. Under non-uniform actions such as wind and snow, bending induces tensile stresses that may lead to cracking. The analyzed configuration corresponds to a triangular shell (15 m span, 4.8 m height) without reinforcement or prestressing, with failure defined as the exceedance of tensile resistance. To enable reliability evaluation, a surrogate-based framework was implemented. Finite element simulations were combined with an artificial neural network (ANN) trained to predict the maximum principal tensile stress under varying load combinations. Monte Carlo simulation, First-Order Reliability Method (FORM), and FORM-based importance sampling were applied to estimate failure probabilities under stochastic wind, snow, and self-weight actions. Results showed consistent reliability indices across methods. Shells with mean flexural tensile strength above 20 MPa satisfied the target reliability index 4.7, while importance sampling significantly reduced computational effort compared to Monte Carlo simulation. The proposed framework demonstrates the applicability of machine-learning-based reliability assessment for free-form concrete shells.

Keywords: structural reliability, machine learning, concrete shells, neural network.

1. Introduction

Concrete shell structures achieve high structural efficiency through geometric form resistance, enabling slender configurations with reduced material consumption. Recent advances in prefabrication, high-performance materials, and prestressing have renewed interest in their application (Hawkins et al., 2016; Li, 2022).

Within this context, the PRESHELL project (Prefabricated Ultra-Thin Concrete Shells) developed a prefabricated funicular shell with triangular geometry in Ílhavo, Portugal.

Previous investigations addressed structural behaviour (Cardoso et al., 2024), prestressing layouts (Gomes et al., 2025), connection systems (Cavaco et al., 2022; Fernandes et al., 2024), construction strategies (Fernandes et al., 2025) and eco-UHPC with flexural tensile strength around 40 MPa (Costa et al., 2025). However, the probabilistic safety of such shells under environmental actions has not yet been quantified (Cavaco et al., 2013).

Although membrane behaviour governs uniform loading, non-uniform wind and snow induce bending and tensile stresses (Cardoso et al., 2024). In unreinforced thin shells, cracking is controlled by flexural tensile strength, and partial safety factors may not capture uncertainty in free-form geometries.

To address these limitations, a surrogate-based probabilistic framework combining numerical simulations and machine-learning was adopted.

Failure probabilities were estimated using Monte Carlo simulation, the First-Order Reliability Method (FORM), and FORM-based importance sampling (Haldar & Mahadevan, 2000).

The analysis considered the unreinforced PRESHELL prototype (Fig. 1), excluding prestressing and connection effects, with failure defined as exceedance of flexural tensile resistance.

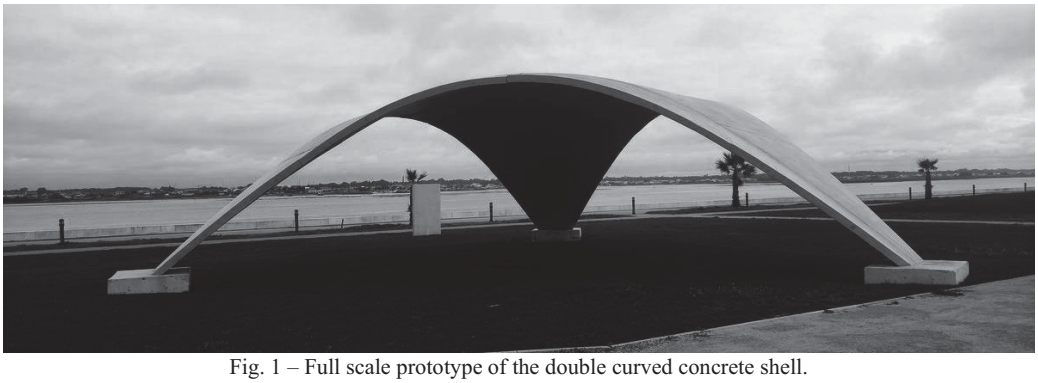

Fig. 1 – Full scale prototype of the double curved concrete shell.

2. Methodology

The reliability analysis of the thin concrete shell combined numerical simulations with machine learning, using Monte Carlo framework to estimate failure probability. This ANN-based approach reduces the number of finite element evaluations required for reliability assessment (Chojaczyk et al., 2015; Hurtado & Alvarez, 2001). The procedure followed the steps described in the following subsections.

2.1. *Problem Definition and Limit State Function*

The objective of the reliability analysis was to estimate the probability of failure of the concrete shell. Due to the non-uniform distribution of snow and wind actions, the shell is subjected to bending effects. Therefore, failure was defined as the condition in which the tensile stress at the top or bottom surface of the concrete shell exceeds its flexural tensile strength.

Accordingly, the ultimate limit state function was defined as expressed in Eq. (1).

$$Z = f_{ct} - \sigma_1(g, s, w, t, \alpha) \quad (1)$$

The stress (σ_1) was expressed as a function of the permanent load of self-weight (g), the variable loads of snow (s) and wind (w), the shell thickness (t) and the wind incidence angle (α). Concrete compressive strength was not considered, as its value was significantly higher than the compressive stresses induced by the evaluated loads (Cardoso et al., 2024).

2.2. *Characterization of Random Variables*

Random samples were generated according to Eurocode recommendations and Joint Committee on Structural Safety (JCSS) probabilistic models. The random variables considered were the permanent load of self-weight (g), the variable loads of snow (s) and wind (w) and the concrete flexural tensile strength (f_{ct}). Shell thickness (t), coefficient of exposure (c_e) and wind incidence angle (α) were treated as deterministic.

2.3. *Unit Load Numerical Simulations*

Given the limited nonlinear residual strength of the shell (Cardoso et al., 2024), the structural response was assumed to be predominantly linear, allowing the superposition. Unit-load simulations were performed in ABAQUS (Dassault Systèmes, n.d.) for each load type. The stress components (σ_{11}, σ_{22}, σ_{12}) were extracted at the top and bottom surfaces of all shell elements. This was repeated for each combination of thickness, wind angle and terrain category.

For each load combination, stresses were scaled by the load magnitudes as expressed in Eq. (2), (3) and (4). For wind loading, scaling considered the square of the wind velocity, consistent with peak dynamic pressure.

$$\sigma_{11,n} = \sigma_{11,g} \cdot g_n + \sigma_{11,s} \cdot s_n + \sigma_{11,w,\alpha} \cdot c_e \cdot w_n^2 \quad (2)$$

$$\sigma_{22,n} = \sigma_{22,g} \cdot g_n + \sigma_{22,s} \cdot s_n + \sigma_{22,w,\alpha} \cdot c_e \cdot w_n^2 \quad (3)$$

$$\sigma_{12,n} = \sigma_{12,g} \cdot g_n + \sigma_{12,s} \cdot s_n + \sigma_{12,w,\alpha} \cdot c_e \cdot w_n^2 \quad (4)$$

This linear combination of stresses enabled estimation of the maximum principal stress (σ_1) in each element of the numerical model, according to Eq. (5), and the maximum value

among all elements was taken as the maximum principal stress for each load combination.

$$\sigma_{1,n} = \frac{\sigma_{11,n} + \sigma_{22,n}}{2} + \sqrt{\left(\frac{\sigma_{11,n} - \sigma_{22,n}}{2}\right)^2 + \sigma_{12,n}^2} \quad (5)$$

2.4. *Neural Network Training*

A neural network was implemented in Python (Python Software Foundation, 2022) using the TensorFlow (2015) to predict the maximum principal stress (σ_1) for a given load combination. The problem was formulated as a supervised regression task in machine learning, mapping the input parameters (loads, thickness, exposure coefficient, and wind incidence angle) to the corresponding stress response (Table 1).

Table 1 - Regression problem: inputs and outputs.

Inputs			Outputs
Loads	Self-weight	g	Maximum Principal Stress σ_1
	Snow	s	
	Wind	w	
Thickness		t	
Coefficient of exposure		c_e	
Wind incidence angle		α	

The training dataset was generated using a hybrid strategy: 95% of the samples were drawn from the probabilistic distributions of the variables, while 5% from Latin Hypercube Sampling (LHS) to ensure input domain coverage. Approximately 95% of the samples were used for training and 5% for validation.

The target σ_1 values were obtained through stress superposition (Eqs. (2)- (4)) and principal stress computation Eq. (5). The Mean Squared Logarithmic Error (MSLE) was adopted as the training loss function, providing higher sensitivity to relative errors in targets with very small magnitudes. Model performance was evaluated using the coefficient of determination (R^2).

2.5. *Large-Scale Monte Carlo Simulation*

After training, the neural network was used to estimate stresses for a large number of load combinations. The required number samples was estimated based on Eq. (6) (Haldar & Mahadevan, 2000), where P_f is the target failure probability and δ is the coefficient of variation of the failure probability.

$$N \geq \frac{1 - P_f}{P_f \cdot \delta^2} \quad (6)$$

The number of samples N corresponds to the number of simulations performed for each configuration defined by a shell thickness, a wind incidence angle and a terrain category.

The overall probability of failure was computed as the ratio of failing samples (N_f) to the total number of Monte Carlo samples (N) as expressed in Eq. (7).

$$P_f = P(\mathrm{Z} \leq 0) \approx \frac{N_f}{N} \quad (7)$$

2.6. *Importance Sampling Based on FORM*

For configurations with very low failure probabilities, a crude Monte Carlo approach would require a large number of simulations, due to both the rarity of failure events and the coefficient of variation of the failure probability. Therefore, importance sampling based the FORM (Haldar & Mahadevan, 2000) was adopted.

FORM was first used to identify the Most Probable Point (MPP) of failure for each configuration, defined as the point on the limit-state surface with minimum distance to the origin in the standard normal space.

An auxiliary sampling density was constructed by preserving the original probabilistic models of g, s, w and f_{ct}, while shifting their means to the corresponding MPP coordinates g^*, s^*, w^* and f_{ct}^*. Each sample was assigned an importance weight (Eq. (8)) to correct for the biased sampling.

$$w_i = \frac{f_g(g_i) \cdot f_s(s_i) \cdot f_w(w_i) \cdot f_{f_{ct}}(f_{ct,i})}{h_g(g_i) \cdot h_s(s_i) \cdot h_w(w_i) \cdot h_{f_{ct}}(f_{ct,i})} \quad (8)$$

Where $f_x(\cdot)$ and $h_x(\cdot)$ denote the original and auxiliary probability density functions, respectively.

The failure probability was estimated using a weighted importance sampling estimator. For a total number of samples N, the failure probability was computed according to Eq. (9).

$$P_f \approx \frac{1}{N} \sum_{i=1}^{N} \prod(Z_i \leq 0) \cdot w_i \quad (9)$$

Where $\prod$ denotates the indicator function assuming 1 if $Z_i \leq 0$, or 0 if $Z_i > 0$.

3. Case Study

3.1. *Funicular shell: Geometry and Loading*

The shell geometry was defined through a nonlinear form finding method (Sá Marques et al., 2019) resulting in the equilibrium shape of an equilateral triangular membrane with 15 meters span, subjected to its self-weight and supported at three points. The shell height was defined as 4.8m by architectural criteria of the PRESHELL project (Fig. 2).

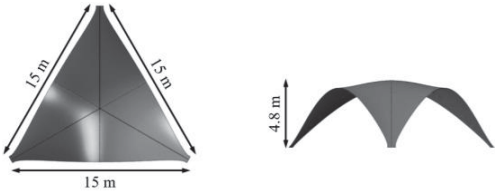

Fig. 2 – Case study triangular shell: (a) Top view; (b) front view.

With 120mm thickness, the thickness-to-span ratio (t/L) of 1/125, classified the structure as a thin shell (Eisenbach, 2017; Ramaswamy, 2019). Following Cardoso et al. (2024), non-uniform snow and wind loads generated significant bending moments and tensile stresses, these critical actions were considered with the self-weight.

The snow load (EN 1991-1-3, 2009), according to its location (Zone 2, altitude 10 m), corresponded to a characteristic value at the ground level (s_k) of 0.2 kN/m^2, shape coefficients were adapted from cylindrical roofs (ter Maten, 2011), with thermal and exposure coefficients equal to unity. The adopted drifted distribution is shown in Fig. 3(a).

The wind load (EN 1991-1-4, 2010, Part 1), according to its location in a coast zone (Zone B, Terrain 0), resulted in a basic wind velocity of 30 m/s. At the top of the shell, the corresponding characteristic peak dynamic pressure is approximately 1.46 kN/m^2. Pressure coefficients were determined through wind tunnel tests on a 1:5 scale model (Teixeira et al., 2016) and converted into simplified distributions suitable for ABAQUS, as illustrated in Fig. 3(b). Positive coefficients correspond to compression, while negative coefficients correspond to suction.

The wind direction in Fig. 3(b), combined with drifted snow Fig. 3(a), produced the highest maximum principal stress.

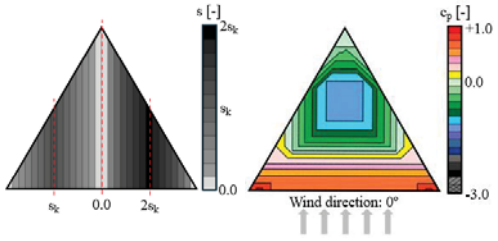

(a) (b)

Fig. 3 – Case study triangular shell: (a) drifted snow load distribution; (b) pressure coefficients for the two wind incidence angles.

3.2. *Numerical model*

A numerical model was developed in ABAQUS to perform the unit-load analysis for stress superposition. Assuming linear behaviour, the concrete was modelled as linear elastic ($E = 39\ GPa, \nu = 0.2$) corresponding to C60 concrete (Model Code, 2010). The model geometry followed section 3.1 with 120 mm thickness. The numerical model was discretized using S3 general-purpose shell elements. The final mesh comprised 10500 elements (Fig. 4). Units loads consisted of: self-weight of 1 kN/m^3; drifted snow with peak intensity of 2 kN/m^2; and wind pressure corresponding to a wind velocity of 1 m/s was 1.62 N/m^2 (Fig. 5).

(a) (b)

Fig. 4 – Numerical model developed in ABAQUS.

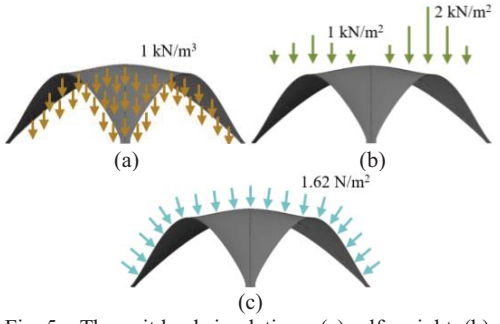

Fig. 5 – The unit load simulations: (a) self-weight; (b) snow load; (c) wind pressure on the external surface.

4. Failure probability assessment

4.1. *Target reliability index*

The structure was classified as CC2 (RC2) according to (EN 1990, 2001). For ultimate limit states and a one-year reference period, a target reliability index β of 4.7 was adopted, corresponding to a failure probability of approximately 10^{-6}. Based on Eq. (6), and assuming a coefficient of variation (δ) of 0.3, the required number of Monte Carlo samples was approximately 10^7.

4.2. *Probabilistic Characterization of Variables*

Self-weight, snow load, wind velocity and concrete flexural tensile strength were modelled as Gaussian, Gamma, Gumbel, and Lognormal variables, respectively, following JCSS recommendations (JCSS: 2.1, 2001; JCSS: 2.12, 2001; JCSS: 2.13, 2001; JCSS: 3, 2002).

Table 2 - Random variables distributions.

Variable	Distribution	Mean / Characteristic value	COV
Self-weight $g\ [kN/m^3]$	Gaussian (μ, σ)	$\mu = 24$	0.03
Snow load $s_k\ [kN/m^2]$	Gamma (k, θ)	$s_k \in \{0.2, 1, 2, 3, 4, 5\}$	2.0
Wind velocity $w\ [m/s]$	Gumbel (μ, β)	$w = 30$	0.3
Tensile strength $f_{ct}\ [MPa]$	Lognormal (μ, σ)	$f_{ct} \in \{2.5, 5, 10, 20, 30, 40\}$	0.3

The self-weight was defined with mean value of 24 kN/m³ and a COV of 0.03, resulting in a standard deviation of 0.72 kN/m³. The ground snow load characteristic values ranging from 0.1 to 5 kN/m² were adopted, with a COV of 2.0, since higher variability is associated with lower altitudes and reduced snow incidence (Pietro Croce et al., 2021). The basic wind velocity was modelled with a characteristic value of 30 m/s and a COV of 0.30. The snow and wind load were defined by characteristic values, corresponding to a return period of 50 years.

Given the dominance of bending effects under non-uniform loading over direct tensile stresses (Cardoso et al., 2024), the flexural tensile strength was adopted as the resistance parameter. The UHPCFR developed for the concrete shell was characterized experimentally by Costa et al. (2025), which indicated a mean flexural tensile strength of 42 MPa at 150 days, attributed to the inclusion of steel fibers.

To assess sensitivity, tensile strength values between 2.5 and 40 MPa were considered. In the absence of experimental data for these values, a COV of 0.30 was adopted (JCSS: 3, 2002). Table 2 resumes the random variables distributions and the range of values adopted.

4.3. *Neural-Network*

The training dataset comprised 50,000 samples generated using probabilistic sampling combined with LHS. Table 3 summarizes the statistical characteristics of the resulting dataset.

Due to the hybrid sampling strategy, the sample statistics did not match the mean and standard deviation of the original probability distributions. The variables $\sigma_{1,top}$ and $\sigma_{1,bottom}$ refers to the maximum principal stresses obtained from stress superposition (Section 2.3).

Table 3 – Statistical characteristics of the neural network training dataset.

Variable	Mean	Standard deviation
$g\ [kN/m^3]$	24.02	0.82
$s_k\ [kN/m^2]$	0.81	2.63
$w\ [m/s]$	16.78	6.66
$\sigma_{1,top}[MPa]$	1.42	3.96
$\sigma_{1,bottom}[MPa]$	1.29	4.13

The neural network architecture (Fig. 6) consisted of five input neurons corresponding to the shell thickness (t), wind incidence angle (α), self-weight load (g), snow load (s), and wind velocity (w), two fully connected hidden layers with 64 neurons each and one output neuron of the predicted maximum principal stress (σ_1).

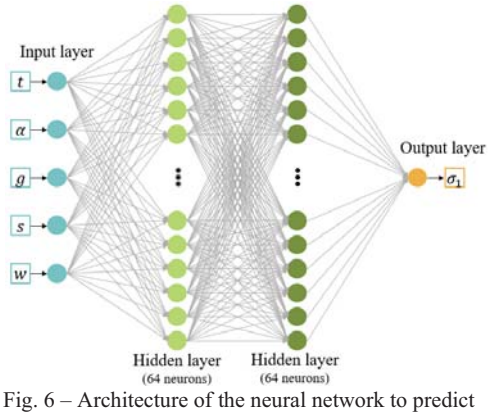

Fig. 6 – Architecture of the neural network to predict the maximum tensile stress.

The final network architecture and training configuration were defined through a trial-and-error process (Barros et al., 2019; Chojaczyk et al., 2015), with early stopping based on validation loss stabilization to avoid overfitting.

Predictions for $\sigma_{1,top}$ and $\sigma_{1,bottom}$ yielded coefficients of determination above 99.99%, MSLE around of 10^{-6}, and MAE below 0.003 MPa, as shown in Fig. 7. The MSLE loss function was adopted to preserve sensitivity to relative errors associated with very small stress values due to the Gamma distribution of the snow load.

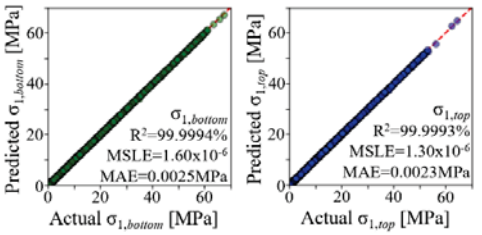

(a) (b)

Fig. 7 – Metrics of the neural network surrogate: (a) σ1,bottom ; (b) σ1,top .

4.4. *Python Algorithm for Reliability Assessment*

The probability of failure was computed using a Python algorithm combining the Monte Carlo simulation with a trained neural network model.

For each thickness and wind incidence angle configuration, random samples of loads and concrete flexural tensile strength were generated. The neural network predicted the maximum principal stress at the shell surfaces, and failure was assumed when the stress exceeded the flexural tensile strength.

The failure probability was estimated as the ratio of failed to total samples. For Monte Carlo (MC) and importance sampling (IS), the failure probabilities were estimated based on Eqs. (7) and (9), respectively.

4.5. *Results of the Failure probability assessment*

4.5.1. *Monte Carlo simulation*

Although the required number of simulations was estimated as 10^7, failure probabilities for average tensile strengths above 20 MPa were significantly low. Therefore, 10^8 simulations were performed. Samples were generated once, it guaranteed tail representation.

Table 4 presents the estimated P_f, β, and COV. The COV increased for very small probabilities. For the concrete with $f_{ct,m}$ of 40MPa with a P_f of 9.06×10^{-8}, the COV exceed unity, which indicated the inefficiency of the Monte Carlo simulation in the rare-event domain comparing to its computational cost.

Only tensile strengths equal to or greater than 20 MPa satisfied the target reliability index of 4.7

Table 4 – Results from the Monte Carlo simulation.

$f_{ct,m}$ $[MPa]$	2.5	5	10	20	30	40
β	2.14	2.83	3.62	4.44	4.90	5.22
P_f	1.61×10^{-2}	2.34×10^{-3}	1.49×10^{-4}	4.40×10^{-6}	4.89×10^{-7}	9.06×10^{-8}
COV	0.002	0.007	0.026	0.151	0.452	1.051

4.5.2. *Importance sampling simulation*

Design points were obtained using FORM for Terrain Category 0 and a ground snow load of 0.2 kN/m². Due to the low snow intensity, failure was wind-dominated, resulting in a single design point for all tensile strengths (Table 5).

Table 5 – Design points obtained from FORM method.

	Design Points					
$f_{ct,m}$ $[MPa]$	g^* $[kN/m^3]$	s^* $[kN/m^2]$	w^* $[m/s]$	f_{ct}^* $[MPa]$	β $[-]$	P_f $[-]$
2.5	23.97	0.0023	30.00	2.02	2.13	1.64×10^{-2}
5	23.98	0.0023	36.71	3.71	2.81	2.34×10^{-3}
10	23.97	0.0023	45.81	6.62	3.60	1.49×10^{-4}
20	23.97	0.0023	57.63	11.30	4.50	4.36×10^{-6}
30	23.97	0.0023	66.22	17.85	4.88	4.84×10^{-7}
40	23.97	0.0023	71.35	22.05	5.22	8.89×10^{-8}

Importance sampling was performed around each design point with sample sizes of 10^3, 10^4 and 10^6, using auxiliary distributions centered at the MPP. The β (Table 6) were stable even for 10^3 samples. The maximum deviation between 10^3 and 10^6 simulations was 3.3% for the lowest tensile strength and below 1% for the remaining cases.

Table 6 – Results from the Importance sampling simulation for different number of samples.

$f_{ct,m}$ $[MPa]$		2.5	5	10	20	30	40
$n = 10^3$	P_f	9.91×10^{-3}	2.01×10^{-3}	1.33×10^{-4}	3.82×10^{-6}	4.06×10^{-7}	1.05×10^{-7}
	β	2.33	2.88	3.65	4.48	4.93	5.19
$n = 10^4$	P_f	9.88×10^{-3}	2.25×10^{-3}	1.48×10^{-4}	7.04×10^{-6}	4.90×10^{-7}	8.98×10^{-8}
	β	2.33	2.84	3.62	4.34	4.90	5.22
$n = 10^6$	P_f	1.21×10^{-2}	2.31×10^{-3}	1.49×10^{-4}	4.08×10^{-6}	4.85×10^{-7}	8.92×10^{-8}
	β	2.25	2.83	3.62	4.46	4.90	5.22

4.5.4. *Comparison*

FORM, Monte Carlo (MC), and importance sampling (IS) produced consistent reliability indices for the analyzed configuration. Given the presence of a single wind-dominated design point, FORM alone would have been sufficient for this case.

Monte Carlo required 10^8 simulations for stable rare-event estimates, whereas importance sampling achieved comparable accuracy with significantly fewer simulations

The comparison between methods is illustrated in Fig. 8, which presents the reliability index obtained for each tensile resistance level. The close agreement between the curves confirms the consistency of the approaches for the present case study.

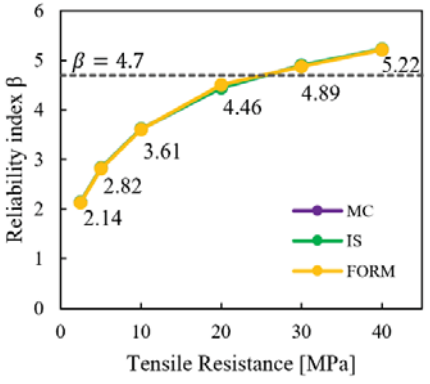

Fig. 8 – Average reliability indices obtained using: Monte Carlo (MC); Importance Sampling (IS); First-Order Reliability Method (FORM).

5. Conclusions

A reliability assessment of an ultra-thin concrete shell subjected to self-weight, snow, and wind was presented, with failure defined by exceedance of the flexural tensile strength.

A hybrid methodology combining finite element simulations, a neural network surrogate model, and probabilistic techniques was implemented. Monte Carlo, FORM, and FORM-based importance sampling were applied and compared. For the analyzed case, all methods yielded consistent reliability indices. However, Monte Carlo required 10^8 simulations for rare events, whereas importance sampling achieved similar accuracy with substantially lower computational effort.

Shells with mean flexural tensile strength above 20 MPa satisfied the target reliability index of 4.7. The prototype constructed in Ílhavo included fibre reinforcement and prestressing, not explicitly considered in the present assessment, where linear behaviour up to the tensile strength limit was assumed.

Although the analyzed scenario represented a simple reliability problem, the neural network was trained over a broad range of thicknesses and loading conditions, enhancing its applicability to other configurations. Future work will extend the analysis to regions with higher snow intensity, where multiple design points may arise, and more advanced structural models incorporating prestressing and indented connections.

Acknowledgement

This work was developed within the scope of the PRESHELL project: POCI-01-247-FEDER-039735, funded by Portugal 2020 through the Lisbon Regional Operational Program, PORLISBOA2020. The authors are grateful for the Portuguese Foundation for Science and Technology (FCT) support through funding the individual research grant 2023.01017.BD.

References

Barros, M., Cavaco, E., Neves, L., & Júlio, E. (2019). Effect of non-structural masonry brick infill walls on the robustness of a RC framed building severely damaged due to a landslide. *Engineering Structures*, *180*, 274–283. https://doi.org/10.1016/j.engstruct.2018.11.027

Cardoso, B., Cavaco, E., Júlio, E., & Tavares, M. E. (2024). Numerical investigation on the behavior of thin concrete shells subjected to nonuniform and asymmetrical loads. *Structural Concrete*, suco.202400532. https://doi.org/10.1002/suco.202400532

Cavaco, E., Almeida, T., & Camara, J. (2022). Seismic behaviour of concrete-to-concrete interfaces subjected to combined shear and bending moment. *Magazine of Concrete Research*, *74*(22), 1150–1164. https://doi.org/https://doi.org/10.1680/jmacr.21.00093

Cavaco, E., Casas, J. R., & Neves, L. (2013). *Quantifying Redundancy and Robustness of Structures*. 78–99. https://doi.org/https://doi.org/10.2749/222137813807018971

Chojaczyk, A. A., Teixeira, A. P., Neves, L. C., Cardoso, J. B., & Guedes Soares, C. (2015).

Review and application of Artificial Neural Networks models in reliability analysis of steel structures. *Structural Safety*, *52*, 78–89. https://doi.org/10.1016/j.strusafe.2014.09.002

Costa, H., do Carmo, R., Rodrigues, T., Rodrigues, A., & Júlio, E. (2025). Development of eco ultra-high performance concrete for the prefabrication of ultra-thin concrete shells. *Structural Concrete*. https://doi.org/10.1002/suco.202400588

Dassault Systèmes. (n.d.). *ABAQUS* [Computer software]. Retrieved https://www.3ds.com/products/simulia/abaqus

Eisenbach, P. (2017). *Processing of Slender Concrete Shells—Fabrication and Installation* [PhD, kassel university press]. ISBN 978-3-7376-0258-7 (print). https://www.uni-kassel.de/ub/index.php?id=39129&h=9783737602587

Eurocode 1: Action on Structures - Part 1-3: General Actions - Snow Loads, Brussels, Brussels, EN 1991-1-3:2009 (2009).

Eurocode 1: Action on Structures - Part 1-4: General Actions - Wind Actions, Brussels, Brussels, EN 1991-1-4:2010 (2010).

Eurocode: Basis of Structural Design, Brussels, Brussels, EN 1990:2001 (2001).

Fernandes, P., Elbashir, D., & Agante, M. (2024). Experimental characterization of indented dry connections for precast double-curved concrete shells. *Structural Concrete*, suco.202400647. https://doi.org/10.1002/suco.202400647

Fernandes, P., Elbashir, D., Cavaco, E., Almeida, N., & Henriques, P. (2025). Production and assembly of ultra-thin concrete shells using prefabrication. *Structural Concrete*, suco.202400708. https://doi.org/10.1002/suco.202400708

Gomes, B., Cavaco, E., Fernandes, P., Júlio, E., & Tavares, M. E. (2025). The effects of post-tension in the behavior of thin funicular concrete shells. *Structural Concrete*. https://doi.org/10.1002/suco.70147

Haldar, A., & Mahadevan, S. (2000). *Probability, reliability and statistical methods in engineering design*. Wiley.

Hawkins, W., Herrmann, M., Ibell, T., Kromoser, B., Michaelski, A., Orr, J., Pedreschi, R., Pronk, A., Schipper, R., Shepherd, P., Veenendaal, D., Wansdronk, R., & West, M. (2016). Flexible formwork technologies – a state of the art review. *Structural Concrete, 6*, *17*, 911–935. https://doi.org/10.1002/suco.201600117

Hurtado, J. E., & Alvarez, D. A. (2001). Neural-network-based reliability analysis: A comparative study. *Computer Methods in Applied Mechanics and Engineering*, *191*(1–2), 113–132. https://doi.org/10.1016/S0045-7825(01)00248-1

JCSS Probabilistic Model Code Part 2 - Load Models: 2.1 Self Weight (2001).

JCSS Probabilistic Model Code Part 2 - Load Models: 2.12 Snow Load (2001).

JCSS Probabilistic Model Code Part 2 - Load Models: 2.13 Wind (2001).

JCSS Probabilistic Model Code Part 3: Resistance Models (2002).

Li, W. (2022). *A review of formwork systems for modern concrete construction*.

Martín Abadi, Ashish Agarwal, Paul Barham, Eugene Brevdo, Zhifeng Chen, Craig Citro, Greg S. Corrado, Andy Davis, Jeffrey Dean, Matthieu Devin, Sanjay Ghemawat, Ian Goodfellow, Andrew Harp, Geoffrey Irving, Michael Isard, Rafal Jozefowicz, Yangqing Jia, Lukasz Kaiser, Manjunath Kudlur, Josh Levenberg, Dan Mané, Mike Schuster, Rajat Monga, Sherry Moore, Derek Murray, Chris Olah, Jonathon Shlens, Benoit Steiner, Ilya Sutskever, Kunal Talwar, Paul Tucker, Vincent Vanhoucke, Vijay Vasudevan, Fernanda Viégas, Oriol Vinyals, Pete Warden, Martin Wattenberg, Martin Wicke, & Yuan Yu, and Xiaoqiang Zheng. (2015). *TensorFlow: Large-scale machine learning on heterogeneous systems* [Computer software]. https://www.tensorflow.org/

Model Code for Concrete Structures 2010, Brussels, Lausanne, Model Code 2010 (2010).

Pietro Croce, Paolo Formichi, & Filippo Landi. (2021). Probabilistic Assessment of Roof Snow Load and the Calibration of Shape Coefficients in the Eurocodes. *Applied Sciences*, *11*. https://doi.org/https://doi.org/10.3390/app11072984

Python Software Foundation. (2022). *Python 3.11* (Version 3.11) [Computer software]. https://www.python.org/

Ramaswamy, G. S. (2019). *Design and Construction of Concrete Shell Roofs (eBook)*. CBS Publishers & Distributions. https://www.amazon.com.br/gp/product/B07R7P1M9J/ref=kinw_myk_ro_title

Sá Marques, T., da Silva, V. D., & Júlio, E. N. B. S. (2019). Form finding of continua shells with lattice spring models. *Engineering Structures*, *200*, 109683. https://doi.org/10.1016/j.engstruct.2019.109683

Teixeira, M., Gomes, M. da G., & da Silva, F. (2016). Ação do vento em estruturas em casca com três apoios. *10º Congresso Nacional de Mecânica Experimental*. 10º Congresso Nacional de Mecânica Experimental.

ter Maten, R. N. (2011). *Ultra High Performance Concrete in Large Span Shell Structures*. Delft University of Technology.